ANN Prediction for Viscous Dissipative Nanofluid Flow on Stagnation Point Flow Over Stretching Sheet

Atifa Latif, Abdaal Hassan, Ayesha Bibi, Muhammad Arsalan
Department of Mathematics, GC University Faisalabad Pakistan
*Correspondence: aatifalatif@gmail.com

Citation| Latif. A, Hassan. A, Bibi. A, Arsalan. M, "ANN Prediction for Viscous Dissipative Nanofluid Flow on Stagnation Point Flow Over Stretching Sheet", IJIST, Vol. 8 Issue.9 pp 3578-3594, October 2026
DOI:
Received| Sep 17, 2026 **Revised|** Sep 24, 2026 **Accepted|** Sep 30, 2026 **Published|** Oct 20, 2026.

This research work presents the combined influence of viscous dissipation and chemical reaction on convective heat and mass transfer in a boundary layer stagnation-point flow of a nanofluid over a stretching sheet. Two types of flow, assisting and opposing, have been considered in this study with the effects of thermophoresis and Brownian diffusion in nanofluid model. The simultaneous impact of viscous dissipation and chemical reaction is of great importance in several practical engineering and thermodynamic processes. Using accurate similarity transformations, the governing nonlinear partial differential equations have been transformed into a set of ordinary differential equations. The bvp4c solver in MATLAB was used to solve these equations numerically with the help of collocation method and obtained the bank of data for artificial neural network (ANN) scheme. A comprehensive investigation was conducted to assess the impact of critical parameters namely, the number of Prandtl particles, Schmidt's numbers, Eckert Number, reaction rate parameter and nanoparticle volume fraction on the velocity, temperature, and concentration profiles. Technique-based neural networks with Levenberg-Marquardt scheme through the backpropagation algorithm has applied on stored data after training. The performance evaluation is such as absolute error, transition state, fitness curves and mean square error. For accurate prediction of physical parameters with reduced computation, The ANN framework was used. The mean squared error of the present study was set to 1.0×10^{-8}, and the Prandtl, Lewis and Schmidt numbers were determined to characterize the thermal and mass transport properties of the fluid. The results from the ANN model have shown strong consistency with those obtained from numerical solutions, providing a reliable approach for investigating complex boundary layer problems.

Keywords: Bvp4c Approach; Artificial Neural Network; Viscous Dissipation; Stagnation Point; Levenberg Marquardt Technique; Nanofluid, Heat Transfer; Boundary Layer; Stretching Sheet.

Main Abbreviations & Parameters	
u and v	Components of velocity
μ	Dynamic viscosity
ρ	Density of fluid
υ	Kinematic viscosity
H	Magnetic field
D_s	Thermal Diffusivity
T	Temperature
$f(\eta)$	Axial velocity profile
(x, y)	Direction co-ordinates
ϕ_1	Scalar potential
a	Distance
Pr	Prandtl number
k	Thermal conductivity
Re	Local Reynold number
γ	Constant
C_f	Skin friction
K	Constant
Nu	Nusselt number
ψ	Stream function
λ	Viscous dissipation parameter
$\theta(\eta)$	Dimensionless temperature profiles
α	Dimensionless distance
T_c	Specific heat capacity
C	Concentration
ANN	Artificial Neural Network
BPLMT	Back Propagation by Levenberg-Marquart Technique
MSE	Mean Square Error

Introduction:

Nanofluids are produced through the mixing of nanoparticles into a simple fluid such as water and have superior thermal conductivity compared to equivalent non-nanofluids. Recently, the use of AI approaches (Artificial Neural Networks (ANN)) has further expanded our knowledge and ability to predict the behavior of nanofluids. Viscous dissipation plays a large role in creating heat in fluid systems. [1] introduced in their study the high impacts of viscous dissipation in nano and microtubes. As the size of the system decreases, viscous effects become more pronounced. Based on this research, [2] used hydromagnetic nanofluid flow over adding flow sheet along with heat change and chemical reaction effects to illustrate that viscous dissipative energy can help to increase thermal energy. Similarly, [3] performed numerical simulations of MHD nanofluid flow and indicated that viscous dissipation has a substantial effect on the great change in the heating boundary layer thickness. Furthermore, [4] conducted a field of microchannels that explains the change in heat because of internal friction and hydromagnetic nanofluid flow through small channels. They found that viscous dissipative nanofluid interacts the influence of flow field coupling with velocity and temperature fields. [5] studied higher-order chemical reactions occurring in electrically conductive MHD (magnetohydrodynamic) nanofluids and reported that the parameters related to the chemical reaction processes greatly affected the concentration distributions as well as the thermal boundary layers of electrically conductive nanofluids.

Chemical reactions are the basis of life and nature, assisting human in various processes as a strong force to sustain in the world. Conversion of food into energy within a living body is also a chemical reaction likewise production of clean fuels and formation of medicines etc. [6] looked at the association between chemicals, radiation, and viscous dissipation on non-linear stretching sheets. For instance, [7] studied the hydromagnetic transport characteristics of non-linear stretching sheets subject to convective heating and slip at the wall. They concluded that surface stretching is important in altering flow results. [8] examined the unsteady MHD nanofluid flow over stretching sheets increasing in heat due to friction inside the sheets. The multiple contributions by researchers particular in field of viscous dissipation study further emphasized the significance of modeling stretching and shrinking sheets. [9] observed the radiative MHD flow of a Bingham nanofluid through mathematical modeling.

Tri-hybrid nanofluid flows are the more complex form of nanofluid flows under combined physical effects which provided a basis for understanding better control of fluid flow. [10] analyzed the influence of chemical reactions on tri-hybrid nanofluid blood flow of stretching surface using the Buongiorno model. They employed the Levenberg–Marquardt neural network algorithm to obtain accurate numerical solutions. Their results revealed that chemical reactions significantly change in heat as well as mass characteristics in nanofluid flow systems. [11] examined the stagnation flow of a nanofluid over a rough surface using a tangent hyperbolic model, considering energy dissipation effects. Results showed enhanced change in heat performance, making the model applicable to various engineering processes involving non-Newtonian nanofluids. [12] examined a nanofluid's particles change in heat through stagnation point with convective heating. Their investigation concentrated on the effects of hybrid nanoparticles on fluid and heat transmission during peristaltic action. The findings demonstrated that the addition of hybrid nanomaterials increases change in heat efficiency and thermal conductivity.

The previous studies revealed that the surface roughness and viscous dissipation significantly affects the velocity and temperature profiles within a fluid model. Continuing the effort, [13] comprehended how turbulence improves thermal energy transmission, heat transport processes in turbulent convection were examined. [14] conducted a thorough review of horizontal convection, scrutinizing the flow and change in heat resulting from non-uniform

surface buoyancy. [15] presented a convective transport theory to improve the estimation of surface fluxes in the atmospheric boundary layer. The study integrates turbulence and convection dynamics, offering a more physically consistent framework for modeling heat, momentum, and moisture fluxes between the surface and atmosphere. [16] advanced this field by examining a hybrid nanofluid with convective heat transfer, radiation, and a permeable stretching/shrinking surface. [17] have provided a stochastic numerical study for a fluid moving over a permeable surface normal to the direction of flow by incorporating stochasticity to represent. Performed [18] have the study the change and impacts on laminar boundary layer properties through a nanofluid in the flow over a stretching sheet and found that addition of nanomaterial increases thermal conductivity, resulting in higher rate of change in heat. Most recently, [19] utilized ANN modeling in Buongiorno nanofluid model on stretching sheets. Moreover, there has been recent interest in applying computational and numerical methods in MATLAB modeling in nanofluids, as seen in [20]. Furthermore, [21] explored how nanoparticles effect the motion of nanofluid over a stretching adding flow sheet and solve the numerical equation using the MATLAB bvp4c.

ANN in fluid mechanics research can obtain the relationship between input parameters and output values by numerical data, experimental data and simulated data. [22] used an ANN model to report an excellent agreement between predicted and experimental results in nanofluid tubes through circular tubes while significantly reducing computational efforts. [23] extended the use of intelligent techniques by examining the viability of nanofluid particles models for estimating the thermophoresis properties of Al2O3–MWCNT/oil nanofluids. An ANN optimization model through the non-dominated sorting genetic algorithm II (NSGA-II) was created by [24] to forecast the ANFIS models outperformed traditional methods in terms of prediction accuracy for the mixture of ethylene glycol and water. Later on [25] further created an ANN integrated model for engineering optimization that effectively captured the nonlinear relationship between operating parameters and ethylene glycol–water-based nanofluid properties. [26] investigated the nanofluid heat transfer model to optimize the effective parameters influencing nanofluid change in heat performance by combining artificial neural networks with genetic algorithms.

The present work examines the dominant effects of chemical reaction and viscous dissipation on boundary layer stagnation point flow across a stretched sheet in a nanofluid with uniform wall temperature, concentration and nanoparticle concentration. The ANN-BPLMT approach based on Levenberg–Marquardt back propagation is used in the present work to forecast the given model utilizing BVP4c-generated solutions of the transformed ODEs as the reference dataset for MATLAB-based neural network training and evaluation. The importance of key parameters involved in the situation is explained and shown through graphs.

Mathematical model of BNFs:

The following points summarize the description of two-dimensional steady, incompressible, laminar and convective with boundary layer flow past a stretched sheet.

- In coordinates system Figure 1 stretching and shrinking sheets represents nanofluid flow on stagnation point (*S*) at ($X = 0; Y = 0$) (the point where flow hit the boundary).
- Fluid hit the surface and spread over the surface. Graph represents the key terms use in this graph like external flow $u_e x = ax$ at point (*T*).
- Sheet Velocity $u_w x = bx$.
- There are some important terms represents by graph in which velocity: $u(x, y)$, temperature: $T(x, y)$, nanofluid volume friction: $\phi(x, y)$, concentration: $C(x, y)$.
- Stretching and shrinking sheets graphs present the fluid flow.

- Parameter $\lambda_c = b/a$ show the either the graph is stretching or shrinking.
- If $\lambda_c = b/a$ is <0 then shrinking and if $\lambda_c = b/a$ is >0 then stretching.
- Free stream condition are: $T = T_\infty$, $\phi = \phi_\infty$, $C = C_\infty$

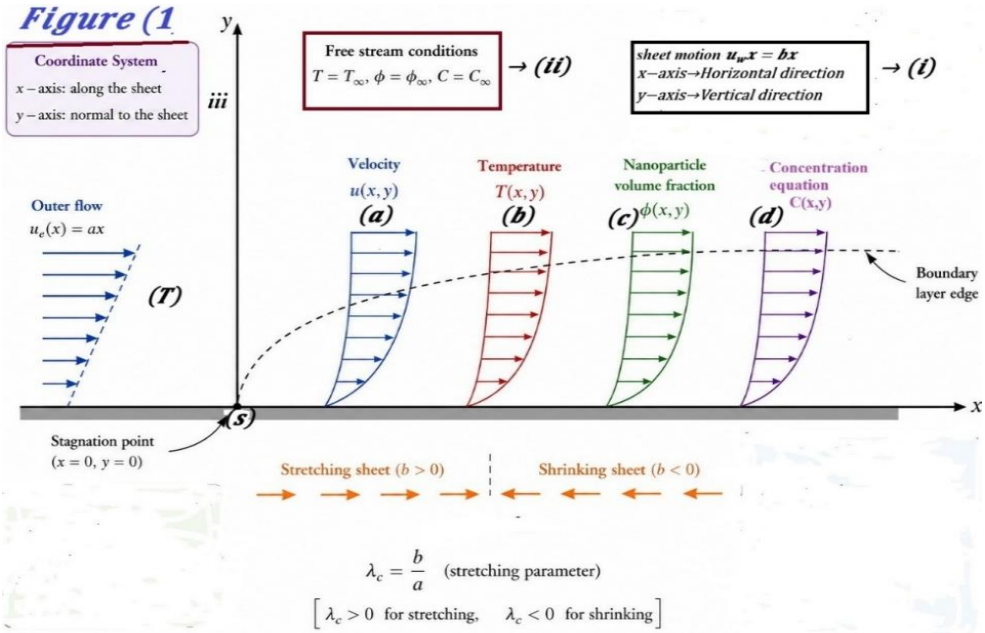

Figure 1. Mathematical representation of physical modelling

The governing equations for stretching sheets with $a > 0$ are as follows:

$$\frac{\partial u}{\partial x} + \frac{\partial v}{\partial y} = 0, \quad (1)$$

$$u\frac{\partial u}{\partial x} + v\frac{\partial u}{\partial y} = u_e(x)\frac{\partial u_e(x)}{\partial x} + \nu\frac{\partial^2 u}{\partial y^2} + (1-\phi_\infty)g\left[\beta_T(T-T_\infty) + \beta_C(C-C_\infty)\right]\frac{(\rho_P - \rho f_\infty)g}{\rho f_\infty} - (\phi - \phi_\infty), \quad (2)$$

$$u\frac{\partial T}{\partial x} + v\frac{\partial T}{\partial y} = \alpha_m\frac{\partial T}{\partial y} + J\left[D_B\frac{\partial \phi}{\partial y}\frac{\partial T}{\partial y} + \frac{D_T}{T_\infty}\left(\frac{\partial T}{\partial y}\right)^2\right] + \frac{\nu}{C_P}\left(\frac{\partial u}{\partial y}\right)^2, \quad (3)$$

$$u\frac{\partial \phi}{\partial x} + v\frac{\partial \phi}{\partial y} = D_B\frac{\partial^2 \phi}{\partial y^2} - \frac{D_T}{T_\infty}\frac{\partial^2 T}{\partial y^2}, \quad (4)$$

$$u\frac{\partial C}{\partial x} + v\frac{\partial C}{\partial y} = D_S\frac{\partial^2 C}{\partial y^2} - k_c(C - C_w), \quad (5)$$

Boundary conditions

$$\left.\begin{aligned} u = u_w(x), v = 0, T = T_w, \phi = \phi_w, C = C_w \text{ at } y = 0 \\ u = u_e(x), \quad T = T_\infty, \quad \phi = \phi_\infty, \quad C = C_\infty \text{ at } y \to \infty \end{aligned}\right\} \quad (6)$$

To convert the PDEs above into nonlinear ODEs, consider the following similarity variables:

$$\eta = \sqrt{\frac{a}{\nu}}y \quad \psi(x,\eta) = \sqrt{a\nu}xf(\eta)\ u = \frac{\partial \psi}{\partial y}, v = -\frac{\partial \psi}{\partial x}$$

$$\theta(\eta) = \frac{T - T_\infty}{T_w - T_\infty}, s(\eta) = \frac{C - C_\infty}{C_w - C_\infty}, \quad \gamma(\eta) = \frac{\phi - \phi_\infty}{\phi_w - \phi_\infty} \quad (7)$$

By using these similarity variables in equations 1 to 5 yielded the following non dimensional system:

$$f'''+ f\,f''- f'^{2}+1+\mathrm{Ri}\,[\theta+Nc.S-Nr.\gamma]=0 \qquad (8)$$

$$\frac{1}{pr}\theta''+ f\theta'+Nb.\theta'\gamma'+Nt.\theta'^{2}+Ec(f'')^{2}=0 \qquad (9)$$

$$\frac{1}{pr}\theta''+ f\theta'+Nb.\theta'\gamma'+Nt.\theta'^{2}+Ec(f'')^{2}=0 \qquad (10)$$

$$\gamma''+Le.f\gamma'+\frac{Nt}{Nb}\theta''=0 \qquad (11)$$

Hence boundary conditions are

$$f(0)=0,\ f'(0)=\varepsilon,\theta(0)=1,\phi(0)=1,\ \text{as}\ \eta=0,$$
$$f'(\eta)\to 1,\theta(\eta)\to 0,\phi(\eta)\to 0\ \text{ for }\ \eta\to\infty, \qquad (12)$$

The expressions representing various physical quantities can be formulated as.

$$\mathrm{Pr}=\frac{\nu_f}{\alpha_f},\ Le=\frac{\nu_f}{D_B},\ Nb=\frac{(JD_B(\phi_w-\phi_\infty))}{\nu},\ Nt=(T_w-T_\infty)\frac{(JDt)}{(\nu T\infty)},\ Ri=\frac{Gr}{\mathrm{Re}^2},$$

$$Sc=\frac{\nu}{Ds},\ Sh_x=\frac{xq_m}{D_B(C_w-C_\infty)},\ Nr=\frac{((\rho_p-\rho f_\infty)\times(\phi_w-\phi_\infty))}{(\rho f_\infty\beta_T(1-\phi_\infty)(T_w-T_\infty)}. \qquad (13)$$

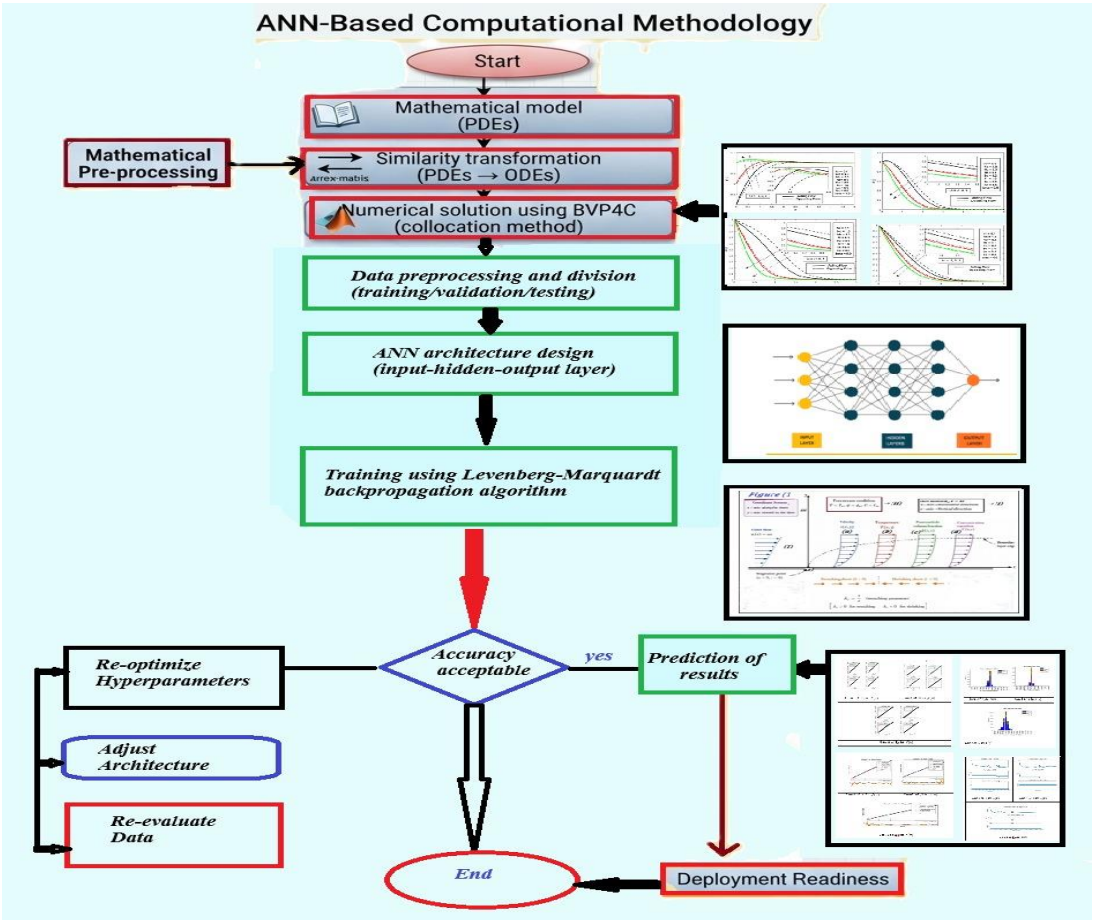

Figure 2. Flow Chart of Problem-Solving Steps with Graphical Solutions

Solution methodology:

The implementation of Artificial neural network with back propagation by Levenberg Marquardt technique referred to as ANN-BPLMT is employed to investigate the BNF model

in accordance with the procedural guidelines. The flow dynamics of BNF model are described by (PDEs) partial differential equations, which are subsequently transformed into a system of (ODEs) ordinary differential equations. To develop the reference dataset characterized by diverse physical properties, these ODEs are resolved utilizing BVP4c function. The reference dataset generated through the BVP4c tool is then integrated with the MATLAB neural networks toolbox to assess the outcomes. The reference dataset comprises with 15% allocated for testing, another 15% for validation, and the remaining portion designated for training purposes. Figure 5 illustrates the neural network architecture for the BNF model, encapsulating all methodological steps undertaken throughout this research investigation. The precision and validation of the proposed BNF model have been assessed through a testing/training-validation methodology within the neural network's framework. To substantiate the efficacy of ANN-BPLMT, regression analysis, histogram evaluations, and mean squared error (MSE) performance metrics are employed. Table 1 delineates the values corresponding to the varying parameters (cases and scenarios) of the nanofluid flows of Buongiorno model.

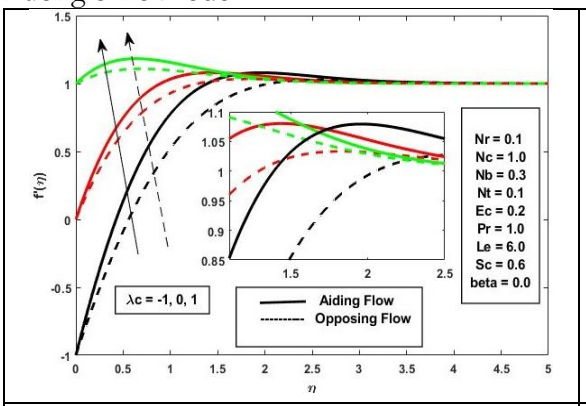

Figure(a) Effect of stretching parameter on velocity profile.

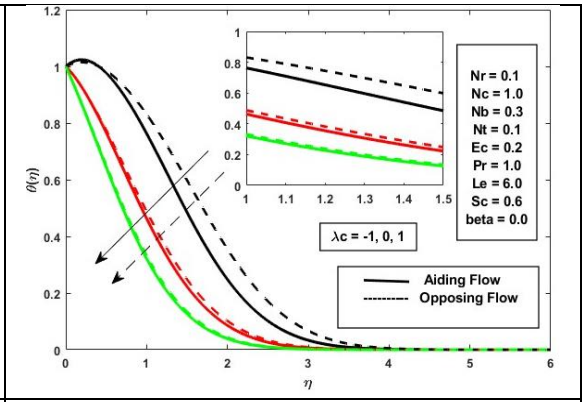

Figure(b) Effect of stretching parameter on Temperature profile.

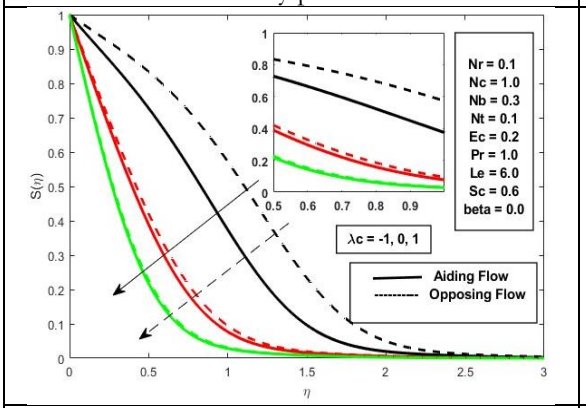

Figure(c) Effect of stretching parameter on Concentration profile

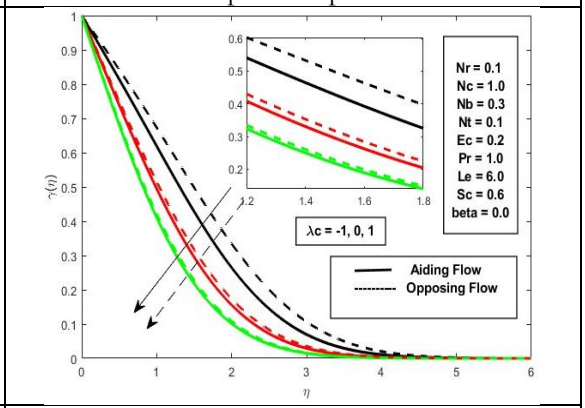

Figure(d) Effect of stretching parameter on Fraction volume

Figure 3. Effects of Various Parameters on Velocity & Temperature Fields

Figure(a) Shows the fluid velocity distribution through $f'(\eta)$ the boundary layer for changed values of the joined convection/buoyancy parameter λ_c =-1,o,1 Increasing λ_c from opposing flow -1 to aiding flow 1 significantly accelerates the fluid motion, introducing a prominent velocity overshoot near the wall due to dominant assisting buoyancy forces. The momentum boundary layer thickness increases with higher values of λ_c, and all curves asymptotically satisfy the far-field boundary condition $f(\infty) \to 1$.

Figure(b) illustrates the impact of the parameter λ_c on the non-dimensional fluid temperature distribution $\theta(\eta)$. As λ_c increases from -1 to1, the temperature curves shift downward, indicating a noticeable reduction in the thermal boundary layer thickness. This cooling effect happens because the enhanced fluid velocity in the aiding flow regime carries heat away from the surface more rapidly via convection.

Figure(c) shows how the fluid concentration decays as you move away from the surface. The distance from the surface is measured by the variable eta on the bottom axis, and the concentration is shown by the variable *S* on the side axis. The solid lines, which represent aiding flow, drop down much faster than the dashed lines, which represent opposing flow. When the stretching parameter λ_c increases from negative one to positive one, all the concentration curves shift downward. This happens because a higher stretching rate speeds up the fluid near the wall, which washes away the concentrated particles and thins the boundary layer.

Figure(d) looks at the volume fraction of the particles, labeled as γ on the side axis, across the distance eta. Just like the previous graph, the solid lines for the aiding flow stay lower and reach zero much faster than the dashed lines for the opposing flow. Increasing the stretching parameter λ_c forces the volume fraction curves to shift downward, which shrinks the layer where these particles are concentrated. Physically, the pulling motion of the stretching surface spreads the particles out more rapidly, and the small cutout box inside the graph zooms in to show this clear separation.

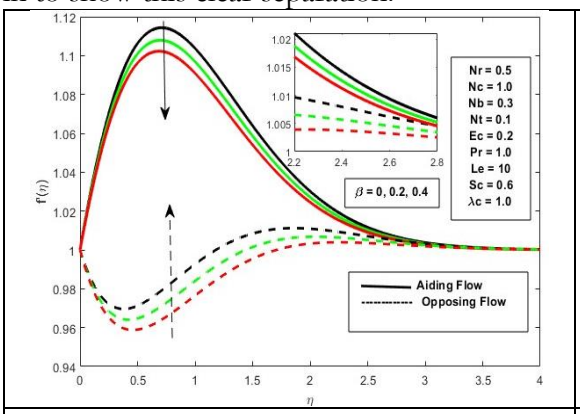

Figure(e) Effect of chemical reaction parameter on velocity profile.

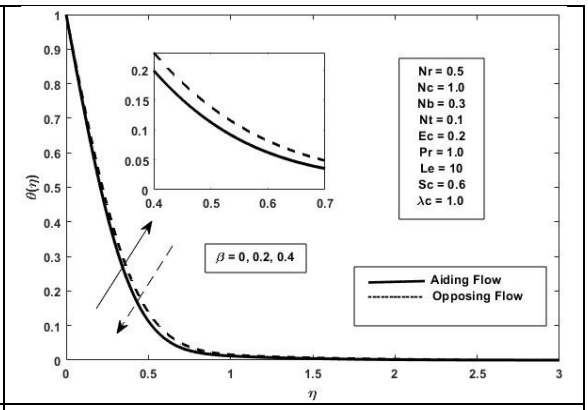

Figure(f) Effect of chemical reaction parameter on Temperature profile

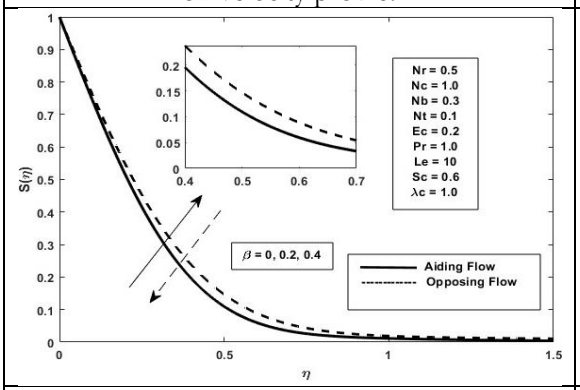

Figure(g) Effect of stretching parameter on Concentration profile

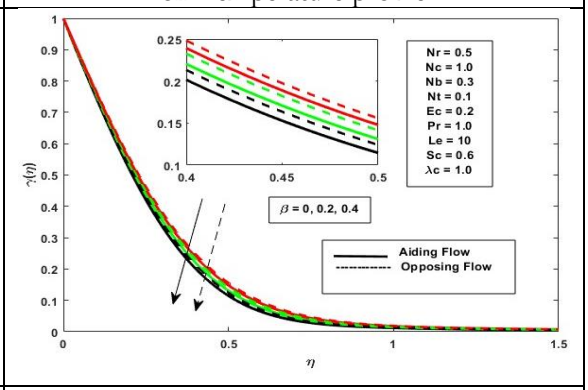

Figure(h) Effect of chemical reaction parameter on volume Fraction profile

Figure 4. Effects of Various Dimensionless Parameters

Figure(e) tracks the fluid speed, labeled as f' on the side axis, as you move away from the wall. In the aiding flow represented by the solid lines, the fluid actually speeds up and

forms a peak before leveling off, while the opposing flow shown by the dashed lines suffers an initial speed drop. As the chemical reaction parameter β increases from zero to zero point four, the peak speed of the aiding flow becomes noticeably lower. This occurs because the chemical reaction weakens the natural buoyancy forces that drive the fluid forward, which ultimately suppresses the fluid speed.

Figure(f) monitors the chemical species concentration, labeled as ϕ on the side axis, across the distance η. Even though the original printed caption contains a mistake by calling this a velocity profile, the axis label confirms it is a concentration graph. There is very little difference between the solid and dashed lines here, meaning the flow direction does not affect this profile very much. However, as the chemical reaction parameter β increases, all the curves shift downward uniformly because a faster reaction consumes and depletes the chemical species near the surface much more quickly.

Figure(g) displays the impact of the chemical reaction parameter on the fluid concentration profile labeled as S on the side axis, against the distance from the surface labeled as η on the bottom axis. Even though the printed caption reads velocity profile, the steady decay from one down to zero confirms it is a concentration field graph. As the chemical reaction parameter beta increases from zero to zero point four, the curves shift slightly downward, and the small cutout box provides a magnified view of this separation. This decrease occurs because a stronger chemical reaction consumes the solute species at a faster rate, thereby thinning the concentration layer near the surface.

Figure(h) shows how the chemical reaction parameter β affects the fraction volume profile labeled as γ on the side axis across the distance η. Just like the previous graph, the caption contains a typo by calling it a velocity profile, but the shape reveals it represents the distribution of a secondary phase like nanoparticles. As the reaction parameter beta increases, the curves move downward, indicating a clear drop in the fraction volume values. Physically, the destructive chemical reaction depletes the particle concentration within the fluid layer, which shrinks the boundary layer thickness for both the aiding flow solid lines and the opposing flow dashed line systems.

ANN Approach:

Artificial numerical computing for the designed ANN- BPLMT is used to examine outcomes of the BNF model described in Equations (06) -(09). The study formulates three distinct scenarios of the BNF model for the concentration, velocity, and temperature profile of the BNF model as displayed in Table 1. The performance, states, and error histograms for each of the five scenarios related to the nanofluid flow cases utilizing the BNF model based on ANN-BPLMT can be observed in figures (3-7), correspondingly.

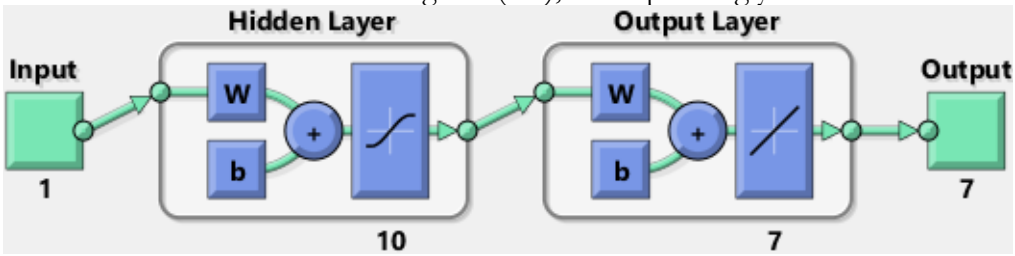

Figure 5. Neuro Structure of BNF-BPLMT

Table 1. Outcomes of ANN-BPLMT for all scenarios of BNF Model.

Scenario	Case	Mean Square Error			Performance	Mu Parameter	Gradient	Epochs	Time
		Training	Validation	Testing					
S-1	**I**	3.6825E-08	2.4216E-08	3.5355E-08	3.68E-08	1.00E-08	1.05E-06	1000	15
	II	1.5287E-08	4.9324E-08	4.8354E-08	1.53E-08	1.00E-09	4.02E-06	1000	09
S-II	**I**	3.6825E-08	2.4216E-08	3.5355E-08	3.68E-08	1.00E-08	1.05E-06	1000	02
	II	3.6825E-08	2.4216E-08	3.5355E-08	3.68E-08	1.00E-08	1.05E-06	1000	12
S-III	**I**	3.6825E-08	2.4216E-08	3.5355E-08	3.68E-08	1.00E-08	1.05E-06	1000	14
	II	1.5287E-08	4.9324E-08	4.8354E-08	1.53E-08	1.00E-09	4.02E-06	1000	09
S-IV	**I**	3.6825E-08	2.4216E-08	3.5355E-08	3.68E-08	1.00E-08	1.05E-06	1000	10
	II	1.5287E-08	4.9324E-08	4.8354E-08	1.53E-08	1.00E-09	4.02E-06	1000	09
S-V	**I**	3.0270E-08	1.7195E-08	2.4542E-08	3.03E-08	1.00E-08	3.55E-05	1000	08
	II	3.4312E-08	2.4147E-08	1.1019E-07	3.43E-08	1.00E-08	2.97E-05	1000	07
S-VI	**I**	1.5105E-08	1.2820E-08	1.5781E-08	1.51E-08	1.00E-08	2.94E-07	1000	12
	II	2.8023E-08	4.2096E-08	5.5538E-08	2.8E-08	1.00E-08	2.14E-06	1000	10
S-VII	**I**	2.7749E-08	2.5583E-08	2.7598E-08	2.77E-08	1.00E-08	7.88E-06	1000	20
	II	2.4502E-08	5.8203E-08	7.4399E-08	2.45E-08	1.00E-08	1.38E-05	1000	17
S-VIII	**I**	9.6241E-08	7.9428E-08	9.6813E-08	9.62E-08	1.00E-08	4.19E-06	1000	18
	II	5.3939E-08	1.3641E-07	1.5737E-07	5.39E-08	1.00E-08	3.04E-05	1000	13
S-IX	**I**	1.5416E-08	9.7814E-09	1.4174E-08	1.54E-08	1.00E-08	4.2E-06	1000	12
	II	3.0585E-08	1.0504E-07	1.3356E-07	3.06E-08	1.00E-08	2.27E-06	1000	10
S-X	**I**	2.1220E-08	1.4581E-08	1.9767E-08	2.12E-08	1.00E-09	1.48E-04	1000	12
	II	3.1702E-08	1.0803E-07	1.3739E-07	3.17E-08	1.00E-08	2.79E-06	1000	10
S-IX	**I**	1.5713E-08	1.5115E-08	1.4311E-08	1.57E-08	1.00E-08	1.8E-06	1000	29
	II	2.0480E-08	2.0052E-08	1.8880E-08	2.05E-08	1.00E-08	1.17E-06	1000	27
S-XII	**I**	1.5713E-08	1.5115E-08	1.4311E-08	1.57E-08	1.00E-08	1.8E-06	1000	29
	II	2.0480E-08	2.0052E-08	1.8880E-08	2.05E-08	1.00E-08	1.17E-06	1000	26

ANN Framework Graphical Images

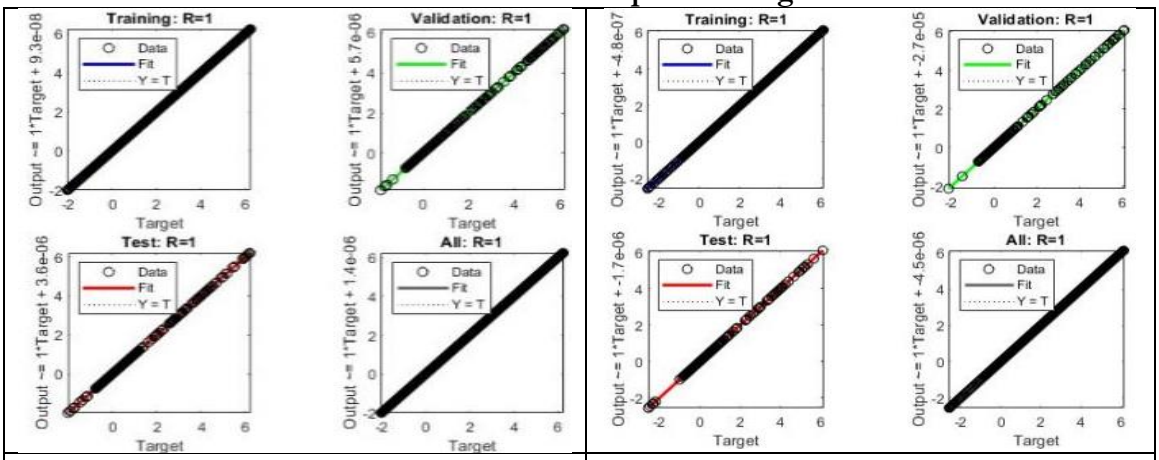

Case-1 of λ_c for $f(\eta)$ | Case-2 **of** β for $f(\eta)$

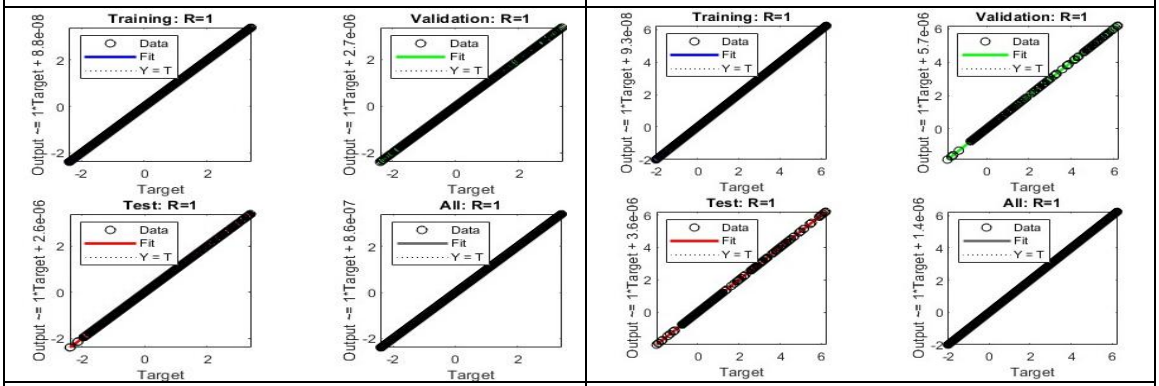

Case-2 of Ec for $f(\eta)$ | Case-1 of λ_c for $\theta(\eta)$

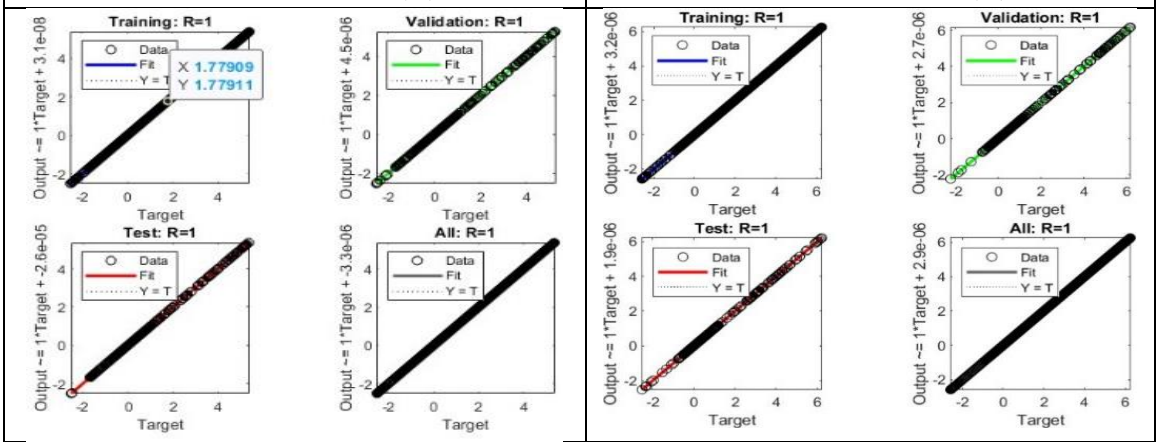

Case-2 **of** β for $\theta(\eta)$ | Case-2 of Ec for $\theta(\eta)$

Figure 6. Regression plots

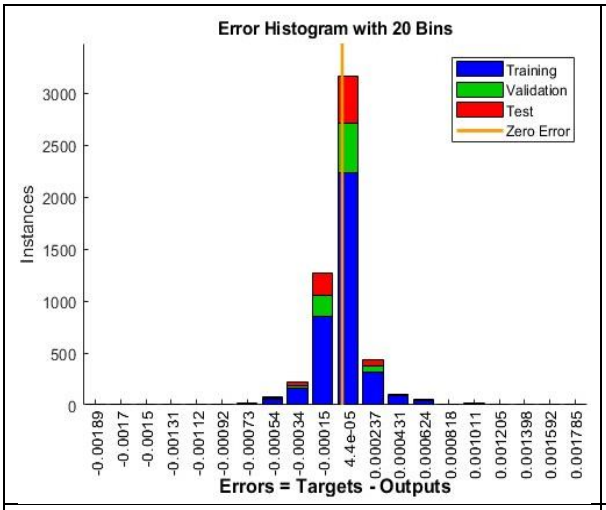

Case-1 of λ_c for $f(\eta)$

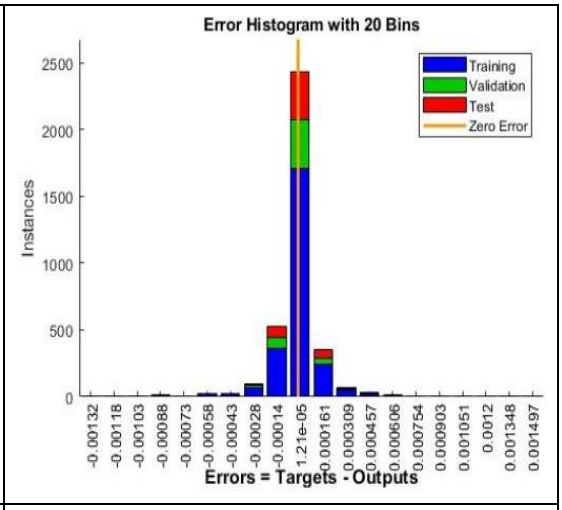

Case-2 **of** β for $f(\eta)$

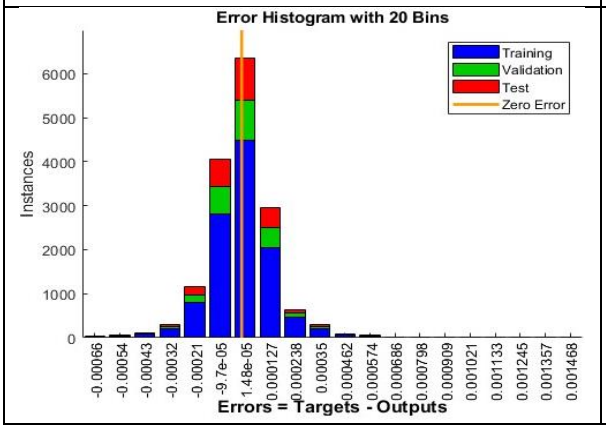

Case-2 of Ec for $f(\eta)$

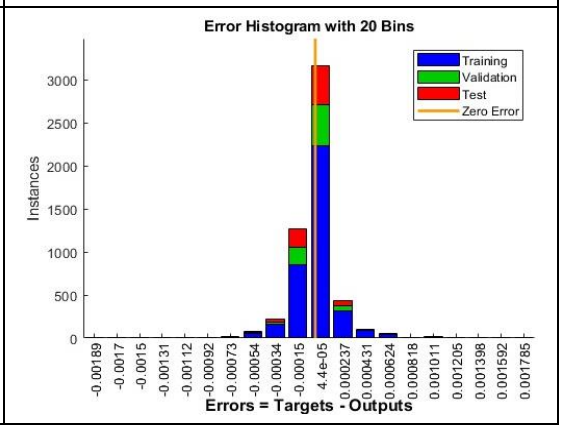

Case-1 of λ_c for $\theta(\eta)$

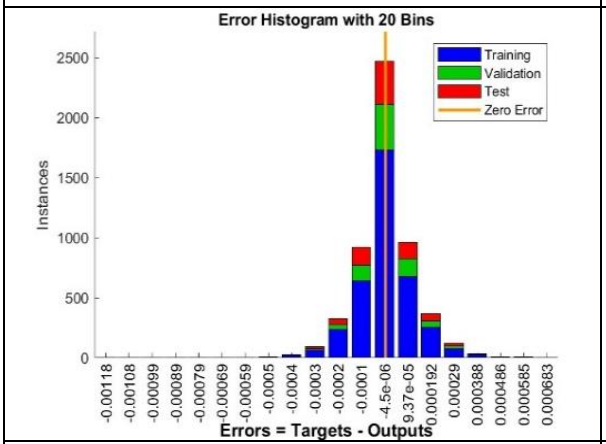

Case-2 **of** β for $\theta(\eta)$

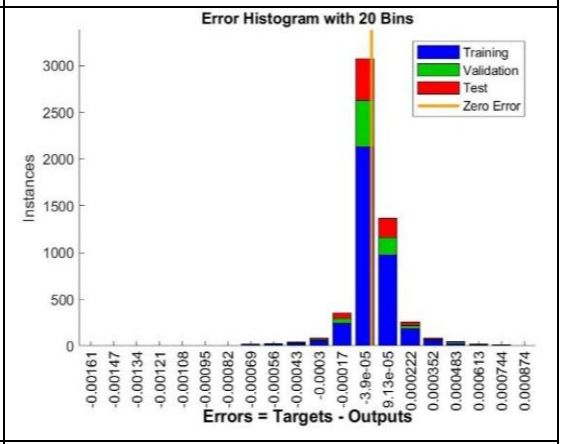

Case-2 of Ec for $\theta(\eta)$

Figure 7. Error Histogram plots

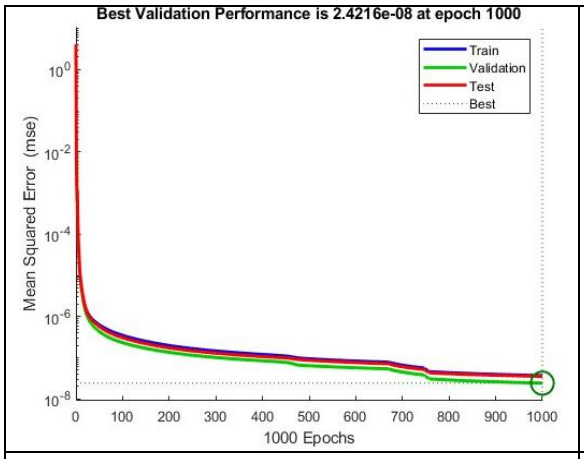

Case-1 of λ_c for $f(\eta)$

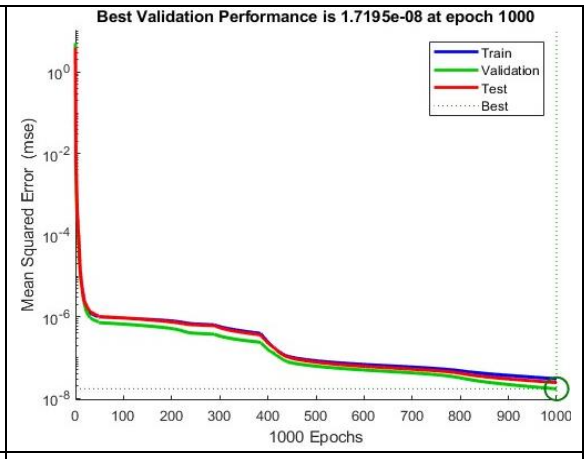

Case-2 **of** β for $f(\eta)$

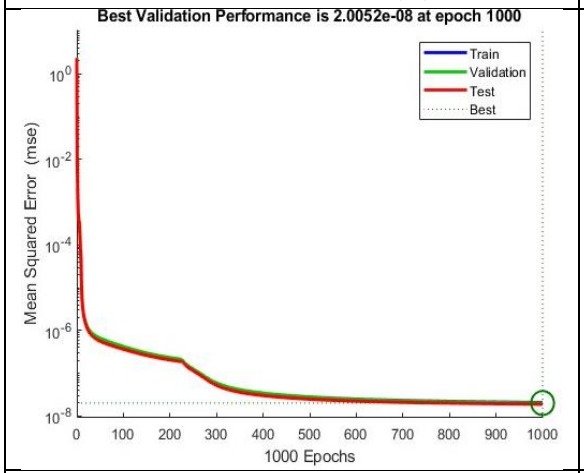

Case-2 of Ec for $f(\eta)$

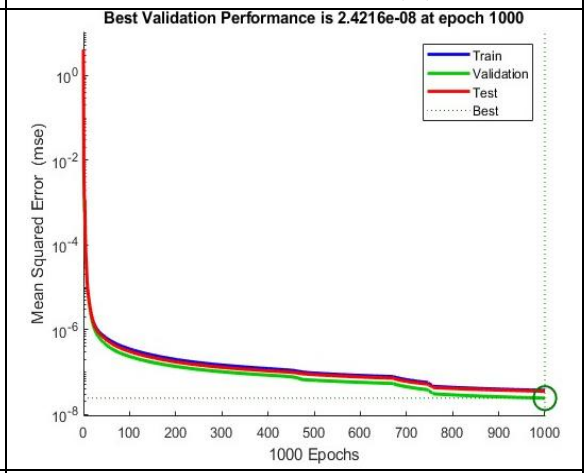

Case-1 of λ_c for $\theta(\eta)$

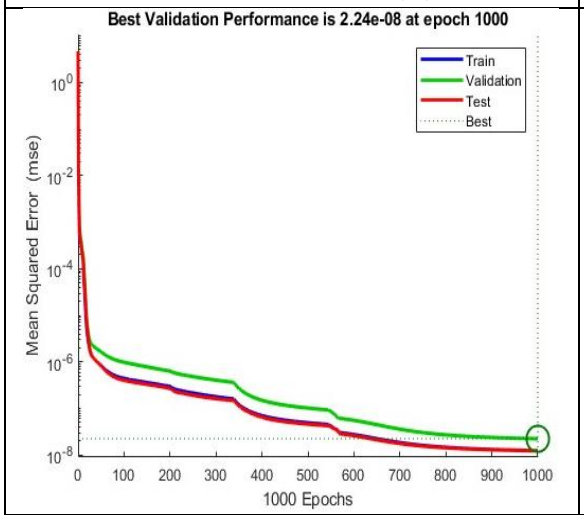

Case-2 **of** β for $\theta(\eta)$

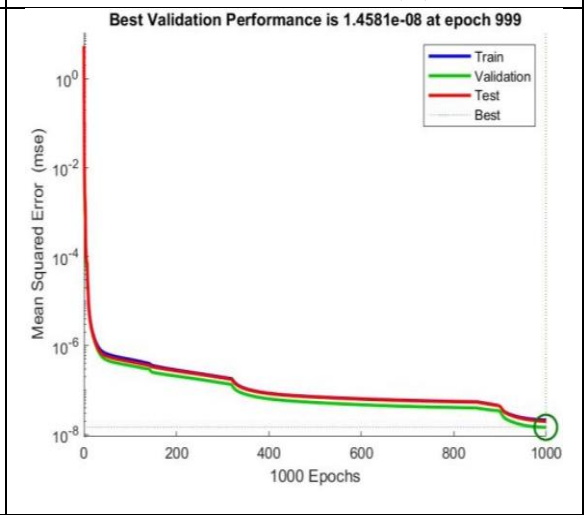

Case-2 of Ec for $\theta(\eta)$

Figure 8. Mean Square Error plots

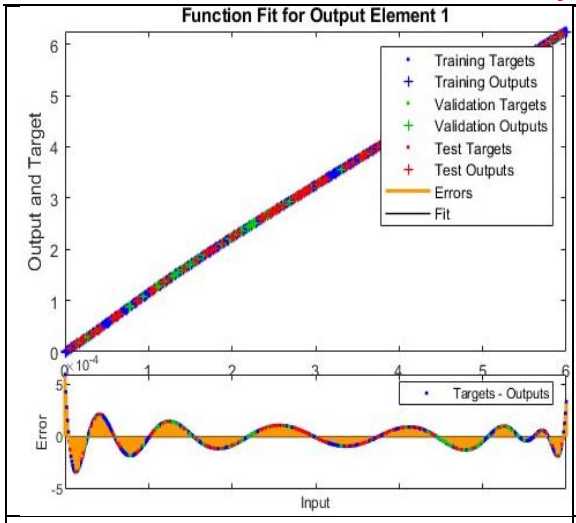

Case-1 of λ_c for $f(\eta)$

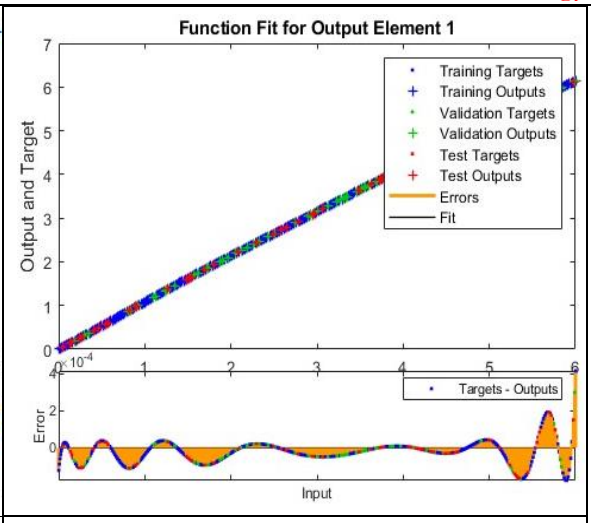

Case-2 **of** β for $f(\eta)$

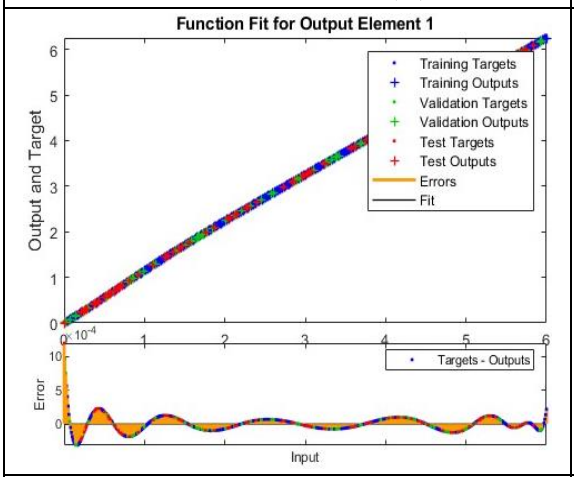

Case-2 of Ec for $f(\eta)$

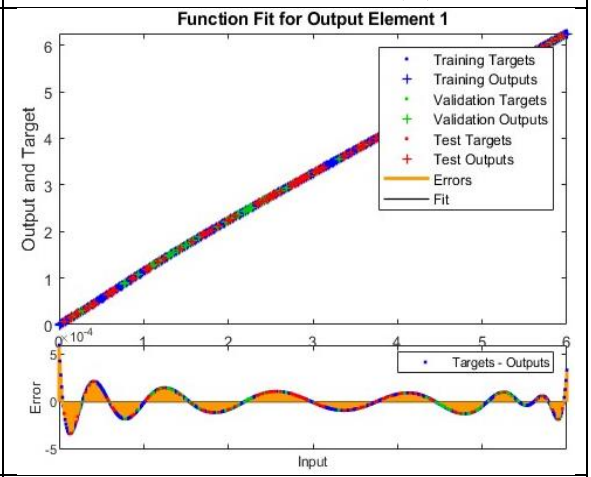

Case-1 of λ_c for $\theta(\eta)$

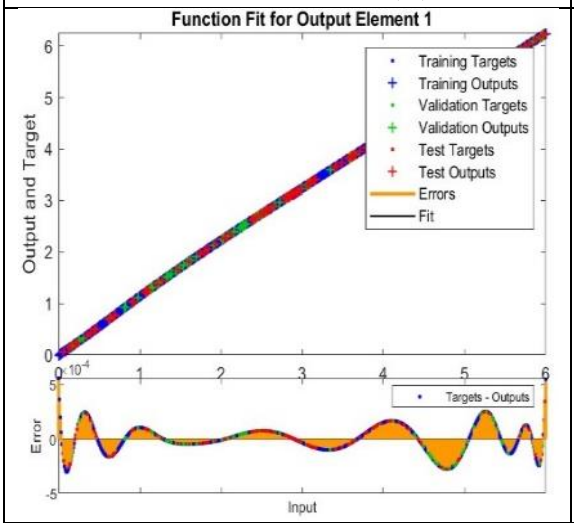

Case-2 of β for $\theta(\eta)$

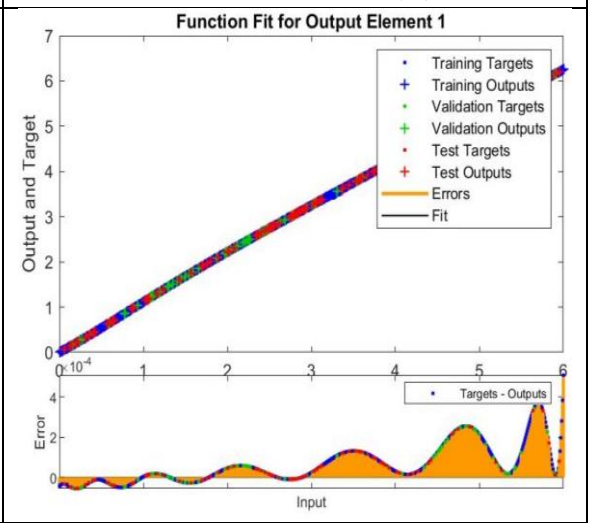

Case-2 of Ec for $\theta(\eta)$

Figure 9. Fitting Curve plots

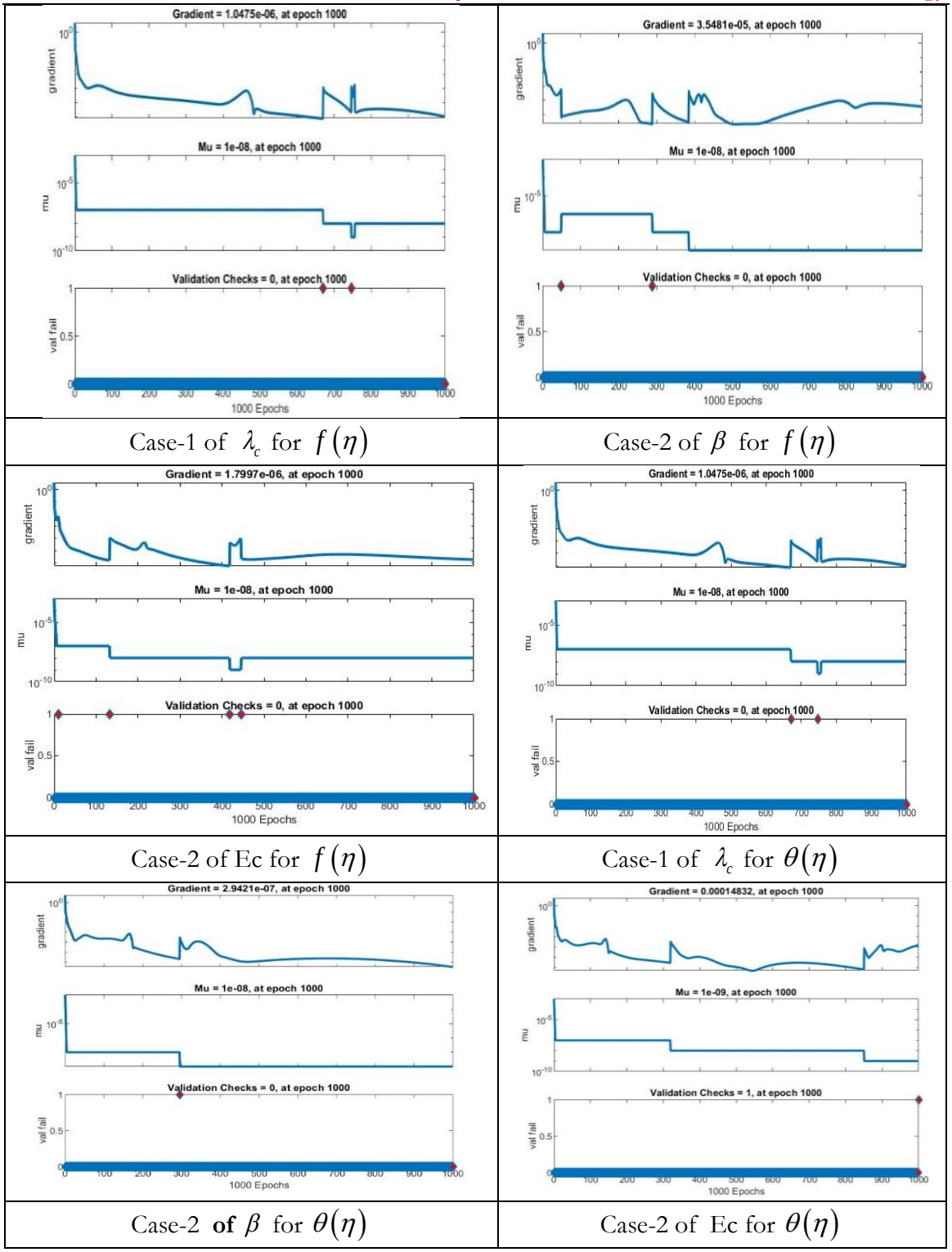

Figure 10. Transition state plots

ANN Framework Discussion

A very close agreement between predicted and actual concentration values is indicated by these plots. The reliability of the ANN model is confirmed by small deviation for concentration prediction which explains the relation between ANN prediction and as well as the target values of velocity profile. Levenberg-Marquardt scheme predicts the velocity with great precision and negligible error with very low square mean square error show the ANN

prediction and actual values difference, it defines the great relationship between temperatures actual results and the predicts results of ANN. Correlations between the results of the temperature and prediction of ANN. Figure 6 developed model of ANN that learn the thermal behavior of Nanofluid confirmed by the testing error, validation and small training.

The histogram (Figure 7) shows that most prediction errors are concentrated near zero, indicating excellent prediction accuracy. This narrow error distribution is consistent with the very small MSE values (Figure 8) reported in the numerical table. A symmetric distribution around zero is exhibited by error histogram with very few large deviations. The accurate and unbiased temperature predictions are provided by ANN is confirmed by this graph. There is a rapid decrease in performance curve and after sometimes reaches a minimum MSE, indicated by fast convergence of the training process. If there is no significant divergence between training and validation errors, it will indicate that overfitting has been successfully avoided. The ANN demonstrates efficient learning by reaching optimal validation performance within a limited number of epochs. The accurate temperature prediction with excellent convergence is confirmed by low-performance plots in Figure 9. The target data is closely matched by the predicted temperature values throughout the entire dataset. The excellent fitting capability and prediction accuracy of the trained ANN is demonstrated by target data. The fit plots for transition state (Figure 10) show that the target velocity values are closely followed by the ANN outputs. The velocity characteristics of the nano fluid are confirmed to be accurately captured by the network, as indicated by the nearly overlapping curves.

Conclusion:

The model nanofluid flow across a stretching sheet is explains in this chapter. Solving the nanofluid particles used the different parameters and AI driven tool for solving the model of nanofluid. In which measure the heat transformation of nanoparticles over a stretching sheet through different parameters.

1. Brownian motion and thermophoresis motion: Brownian motion is the random movements of fluid particles and thermophoresis motion is movement of nanoparticles due to temperature difference.
2. Viscous dissipation parameters are a measure of fluid velocity and its effects on the flow of a fluid.
3. Prandtl number is used to measure in a fluid flow the rate of momentum to heat transfer. It is dimensionless parameter that defines fluid flow to heat transfer.
4. Lewis Number: The nanoparticles concentration profile when decrease the concentration of nanoparticles become thinner in case of Lewis number increases. This happened due to higher Lewis number as compared to lower mass diffusivity within the fluid.
5. Schmidt number: decrease in mass diffusivity to momentum diffusivity because of the concentration profile decrease due to increase in Schmidt number. Because of weak mass transfer the concentration boundary layer become thinner.
6. Buoyancy ratio parameter fluid velocity profile increases due to strong solute buoyancy force the reason of increase in buoyancy ratio parameter. Both the temperature and concentration boundary layer's transport of heat and nanoparticles faster because of reduces in strong convention.

References:

[1] J. Koo and C. Kleinstreuer, "Viscous dissipation effects in microtubes and microchannels," *Int. J. Heat Mass Transf.*, vol. 47, no. 14–16, pp. 3159–3169, Jul. 2004, doi: 10.1016/J.IJHEATMASSTRANSFER.2004.02.017.

[2] P. K. Kameswaran, M. Narayana, P. Sibanda, and P. V. S. N. Murthy, "Hydromagnetic nanofluid flow due to a stretching or shrinking sheet with viscous dissipation and chemical reaction effects," *Int. J. Heat Mass Transf.*, vol. 55, no. 25–26,

pp. 7587–7595, Dec. 2012, doi: 10.1016/J.IJHEATMASSTRANSFER.2012.07.065.

[3] M. Sheikholeslami, S. Abelman, and D. D. Ganji, "Numerical simulation of MHD nanofluid flow and heat transfer considering viscous dissipation," *Int. J. Heat Mass Transf.*, vol. 79, pp. 212–222, Dec. 2014, doi: 10.1016/J.IJHEATMASSTRANSFER.2014.08.004.

[4] T. W. Ting, Y. M. Hung, and N. Guo, "Field-synergy analysis of viscous dissipative nanofluid flow in microchannels," *Int. J. Heat Mass Transf.*, vol. 73, pp. 483–491, 2014, doi: 10.1016/j.ijheatmasstransfer.2014.02.041.

[5] D. Gopal, S. Saleem, S. Jagadha, F. Ahmad, A. Othman Almatroud, and N. Kishan, "Numerical analysis of higher order chemical reaction on electrically MHD nanofluid under influence of viscous dissipation," *Alexandria Eng. J.*, vol. 60, no. 1, pp. 1861–1871, Feb. 2021, doi: 10.1016/J.AEJ.2020.11.034.

[6] W. Abbas, A. M. Megahed, and E. Fares, "The impact of a chemical reaction on the heat and mass transfer mechanisms in a dissipative and radiative nanofluid flow over a nonlinear stretching sheet," *Sci. Reports 2024 141*, vol. 14, no. 1, pp. 7712-, Apr. 2024, doi: 10.1038/s41598-024-57952-9.

[7] M. J. Uddin, O. A. Bég, and N. Amin, "Hydromagnetic transport phenomena from a stretching or shrinking nonlinear nanomaterial sheet with Navier slip and convective heating: A model for bio-nano-materials processing," *J. Magn. Magn. Mater.*, vol. 368, pp. 252–261, Nov. 2014, doi: 10.1016/J.JMMM.2014.05.041.

[8] G. C. Yanhai Lin, Liancun Zheng, Xinxin Zhang, Lianxi Ma, "MHD pseudo-plastic nanofluid unsteady flow and heat transfer in a finite thin film over stretching surface with internal heat generation," *Int. J. Heat Mass Transf.*, vol. 84, pp. 903–911, 2015, doi: https://doi.org/10.1016/j.ijheatmasstransfer.2015.01.099.

[9] Z. Nisar, B. Ahmed, A. Aziz, K. Muhammad, H. A. E. W. Khalifa, and I. Ahmad, "Mathematical modeling and analysis for radiative MHD peristaltic flow of Bingham nanofluid," *ZAMM Zeitschrift fur Angew. Math. und Mech.*, vol. 104, no. 11, p. e202300840, Nov. 2024, doi: 10.1002/ZAMM.202300840

[10] M. Jawad *et al.*, "Chemical reaction impact on Buongiorno model for trihybrid nanofluid blood flow in a squeezed porous channel using the Levenberg–Marquardt neural network algorithm," *Results Eng.*, vol. 25, p. 104252, Mar. 2025, doi: 10.1016/J.RINENG.2025.104252.

[11] M. Alrehili, "Stagnation flow of a nanofluid with rough surface and energy dissipation: A tangent hyperbolic model with practical engineering uses," *Results Eng.*, vol. 26, p. 104825, Jun. 2025, doi: 10.1016/J.RINENG.2025.104825.

[12] T. Hayat, S. Amjad, Z. Nisar, and A. Alsaedi, "Peristalsis of hybrid nanomaterial in convectively heated asymmetric configuration," *J. Therm. Anal. Calorim. 2024 1501*, vol. 150, no. 1, pp. 175–185, Dec. 2024, doi: 10.1007/S10973-024-13790-5.

[13] L. N. Howard, "Heat transport by turbulent convection," *J. Fluid Mech.*, vol. 17, no. 3, pp. 405–432, 1963, doi: 10.1017/S0022112063001427.

[14] G. O. Hughes, R. W. Griffiths, "Horizontal Convection," *AnRFM*, vol. 40, no. 1, pp. 185–208, 2008, doi: 10.1146/ANNUREV.FLUID.40.111406.102148.

[15] R. B. Stull, "A Convective Transport Theory for Surface Fluxes," *J. Atmos. Sci.*, vol. 51, no. 1, pp. 3–22, Jan. 1994, doi: 10.1175/1520-0469(1994)051.

[16] N. S. Wahid, N. M. Arifin, N. S. Khashi'ie, I. Pop, N. Bachok, and E. H. Hafidzuddin, "MHD hybrid nanofluid flow with convective heat transfer over a permeable stretching/shrinking surface with radiation," *Int. J. Numer. Methods Heat Fluid Flow*, vol. 32, no. 5, pp. 1706–1727, Aug. 2021, doi: 10.1108/HFF-04-2021-0263.

[17] M. A. Z. Raja, A. Latif, M. Shamim, K. S. Nisar, and M. Shoaib, "A stochastic

numerical analysis for viscoelastic fluid traversing a permeable perpendicular surface," *Int. Commun. Heat Mass Transf.*, vol. 165, p. 108996, Jun. 2025, doi: 10.1016/J.ICHEATMASSTRANSFER.2025.108996.

[18] W. A. Khan and I. Pop, "Boundary-layer flow of a nanofluid past a stretching sheet," *Int. J. Heat Mass Transf.*, vol. 53, no. 11–12, pp. 2477–2483, May 2010, doi: 10.1016/J.IJHEATMASSTRANSFER.2010.01.032.

[19] M. A. Z. Raja, A. Latif, M. Shamim, K. S. Nisar, and M. Shoaib, "Design of artificial neural network for buongiorno model with nanofluids flow through stretching sheet," *Case Stud. Therm. Eng.*, vol. 69, p. 106054, May 2025, doi: 10.1016/J.CSITE.2025.106054.

[20] S. Suresh and S. R. Shanthi, "Mathematical model of steady incompressible nanofluid for heat transfer applications using MATLAB®," *Micro Nanofluid Convect. with Magn. F. Eff. Heat Mass Transf. Appl. using MATLABÂ®*, pp. 31–58, Jan. 2022, doi: 10.1016/B978-0-12-823140-1.00003-8.

[21] A. Latif, S. Iftikhar, H. Ali, S. Sheraz Asghar, "MatLab Bvp4c Technique to Compute Thermophoresis and Brownian Motion in Nanofluid Flow Over a Transient Stretching Sheet," *Int. J. Innov. Sci. Technol.*, vol. 7, no. 3, pp. 2171–2183, Sep. 2025, doi: 10.33411/IJIST/1554.

[22] B. Vaferi, F. Samimi, E. Pakgohar, and D. Mowla, "Artificial neural network approach for prediction of thermal behavior of nanofluids flowing through circular tubes," *Powder Technol.*, vol. 267, pp. 1–10, Nov. 2014, doi: 10.1016/J.POWTEC.2014.06.062.

[23] I. M. Alarifi, H. M. Nguyen, A. N. Bakhtiyari, and A. Asadi, "Feasibility of ANFIS-PSO and ANFIS-GA Models in Predicting Thermophysical Properties of Al2O3-MWCNT/Oil Hybrid Nanofluid," *Mater. 2019, Vol. 12, Page 3628*, vol. 12, no. 21, p. 3628, Nov. 2019, doi: 10.3390/MA12213628.

[24] M. Hemmat Esfe *et al.*, "Optimization, modeling and accurate prediction of thermal conductivity and dynamic viscosity of stabilized ethylene glycol and water mixture Al2O3 nanofluids by NSGA-II using ANN," *Int. Commun. Heat Mass Transf.*, vol. 82, pp. 154–160, Mar. 2017, doi: 10.1016/J.ICHEATMASSTRANSFER.2016.08.015.

[25] M. Hemmat Esfe, "Designing an artificial neural network using radial basis function (RBF-ANN) to model thermal conductivity of ethylene glycol–water-based TiO2 nanofluids," *J. Therm. Anal. Calorim. 2016 1273*, vol. 127, no. 3, pp. 2125–2131, Aug. 2016, doi: 10.1007/S10973-016-5725-Y.

[26] H. Pourpasha, P. Farshad, and S. Zeinali Heris, "Modeling and optimization the effective parameters of nanofluid heat transfer performance using artificial neural network and genetic algorithm method," *Energy Reports*, vol. 7, pp. 8447–8464, Nov. 2021, doi: 10.1016/J.EGYR.2021.10.121.



Copyright © by authors and 50Sea. This work is licensed under Creative Commons Attribution 4.0 International License.